COMMUNICATION

ADVANCED MATERIALS
www.advmat.de

ADVANCED SCIENCE NEWS
www.advancedsciencenews.com

An Arbitrary Color Light Emitter

Wei-Chun Tan, Yu-Chi Chen, Yi-Rou Liou, Han-Wen Hu, Mario Hofmann, and Yang-Fang Chen**

Light emitting diodes (LEDs) play an important role in our daily lives as lighting sources and information displays, because of their brightness, durability, and high efficiency.[1–5] Many of these applications require the dynamic adjustment of the emission color during device operation. To achieve such a behavior, several LEDs with different emission spectra are commonly integrated into one functional cell, which increases fabrication cost, and limits the achievable resolution.[6–8] To overcome these issues, light emitters with dynamically adjustable emission spectra are required. Currently, dynamic color control can be exerted through adjustment of bias conditions. For example, color modulation can be achieved in complex organic semiconductor heterostructures by adjusting the injection of carriers and confining the injected carriers within one of several emission layers.[9] Alternatively, multifaceted nanostructures such as quantum well nanorods and nanotips provide a route to adjust the carrier pathways by bias conditions, which results in color tunability.[10] Finally, selective emission from certain defect states in partially reduced graphene oxide was shown to produce variable emission spectra.[11] Bias control, however, only offers one adjusting parameter in the color space and is thus similar to varying the color of an incandescent light bulb by changing the lamp power.[12,13] To access the whole chromaticity space, two independent parameters such as hue and saturation are required.

Here we demonstrate the potential of graphene/insulator/semiconductor light emitting transistors for color tunable light emission throughout the whole chromaticity space. The device operating mechanism relies on tunneling from graphene into prominent states in the semiconductor and successive light emission. This process was found to be controllable by bias conditions, i.e., negative bias produced preferential emission from deep-acceptor levels whereas positive bias resulted in bandgap emission. The gating conditions in the employed three-terminal light emitting transistor (LET) architecture modifies the emission spectrum independently of bias conditions. In situ optical spectroscopy reveals that this behavior originates from energy-dependent blocking of tunneling by modulation of the graphene's Fermi level. After adding a downconverting film of quantum dots (QDs), we achieved color tunability over the whole chromaticity space by adjusting bias and gating conditions independently. The potential of this achievement was demonstrated through selective white light emission by proper adjustment of LET operating parameters.

The structure of the fabricated vertical light emitting transistor on sapphire substrate is shown in **Figure 1**a. The top layer of graphene was used to serve as the transparent gate electrode, the middle layer of graphene is the source terminal, and the drain terminal is connected to the p-GaN layer. The 330 nm thickness of SiO_2 film plays as the role of dielectric layer to avoid the leakage current. Meanwhile, the 10 nm SiO2 thin film was used to work as a tunneling barrier. The photoluminescence (PL) spectrum under 325 nm laser exposure at room temperature exhibits a emission peak at 420 nm arising from acceptor impurities as shown in Figure 1b and the peak at 560 nm is due to the emission involving defect transitions.[14,15]

Figure 2a shows the electroluminescence (EL) spectra of the graphene/SiO_2/p-GaN LEDs structure under forward bias (9 V). It could be defined $V_D > 0$ V, $V_S = 0$ V, and then $V_{SD} > 0$ V here. This device exhibits a blue emission originating near the bandedge.[16] When biased in reverse (–12 V) (which means $V_{SD} < 0$ V) the same device shows an additional orange-red emission band around 635 nm. The difference in emission characteristics does not originate from a change in the underlying carrier transport mechanism which can be inferred from the similar trends in the Simmon's plot (Figure 2b). Instead, transport proceeds mainly by tunneling under both biasing conditions as indicated by the good fit to the Simmon's equation:

$$I_{SD} \propto V_{SD}^2 \exp\left(-\frac{4d\sqrt{2m\varphi^3}}{3\hbar e V_{SD}}\right) \quad (1)$$

where d here is the barrier width, φ is the tunnel barrier height, and m is the effective mass of carrier in graphene.[17,18] The observed difference in characteristics can be understood when considering the energy diagrams under different bias conditions. Figure 2c shows the schematic of carrier transport in the energy diagram under forward bias. Under this condition, the bands of p-GaN near SiO_2 layer are bent upward and holes are accumulating at the interface. Under reverse bias, on the other hand, the bands of p-GaN are bent downward and electrons are accumulating. Due to graphene's ambipolar nature electron- and hole-tunneling proceed with similar efficiency and the complementary carrier type to the accumulated charges is provided to facilitate radiative recombination.[19] In the case of hole

W.-C. Tan, Y.-C. Chen, Y.-R. Liou, H.-W. Hu
Graduate Institute of Physics
National Taiwan University
Taipei 106, Taiwan
Prof. M. Hofmann
Department of Material Science and Engineering
National Cheng Kung University
Tainan 70101, Taiwan
E-mail: mario@mail.ncku.edu.tw
Prof. Y.-F. Chen
Department of Physics
National Taiwan University
Taipei 106, Taiwan
E-mail: yfchen@phys.ntu.edu.tw

DOI: 10.1002/adma.201604076

 © 2016 WILEY-VCH Verlag GmbH & Co. KGaA, Weinheim

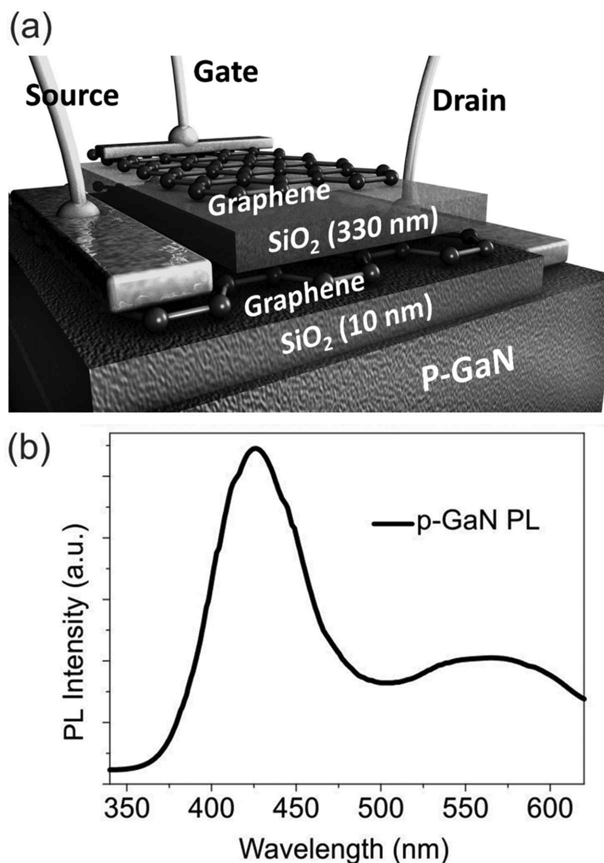

Figure 1. a) Schematic of the device structure. b) Photoluminescence spectrum of p-GaN at room temperature under 325 nm excitation.

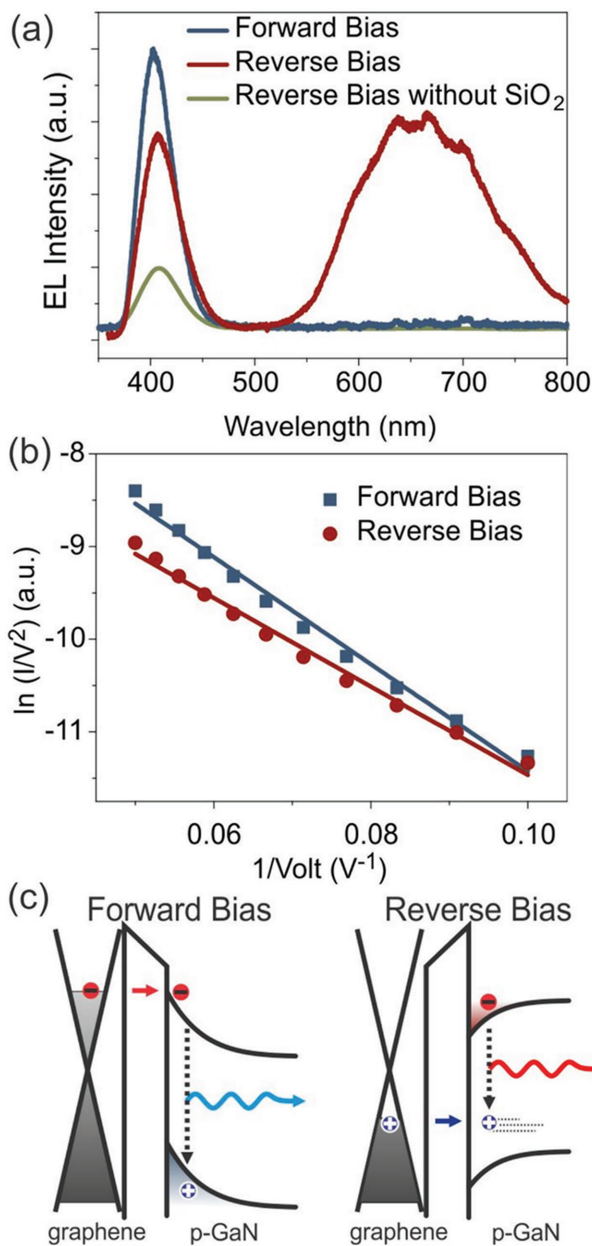

Figure 2. a) Room temperature electroluminescence spectra of graphene/SiO_2/p-GaN LEDs under forward and reverse bias, and reverse bias with and without thin SiO_2. b) Simmons plot under forward and reverse bias, and fit to Equation (1). c) Energy level diagrams of the device under forward and reverse bias.

accumulation under forward bias, electrons are injected from the graphene into the band edge states that then recombine and result in blue emission. For electron accumulation under reverse bias, hole tunneling from graphene can proceed either into states at the band edge or deep acceptor levels which results in an additional emission band and an orange-red emission color.

The presented mechanism is fundamentally different from previously described graphene-based Schottky-barrier emitters where direct tunneling between states in the graphene and the p-GaN is not the dominating transport mechanism. To support this explanation we fabricated another device where graphene is in direct contact with p-GaN without the SiO_2 barrier. This device shows a much weaker EL intensity (Figure 2a) since no electron-accumulation occurs at the interface. Furthermore, no orange-red emission was observed under reverse bias which corroborates the distinction from Schottky emission. We thus find that the biasing conditions control several characteristics of the emission process: As in traditional LEDs, the bias is controlling the emission intensity, but its sign is changing the emission spectrum, i.e., the relative intensity of two emission bands. To manipulate the two bands individually and have access to the whole chromaticity space, a second adjusting parameter is needed. Since the underlying operation mechanism is tunneling transport, the alignment between states in graphene and p-GaN will affect the charge transfer and thus the emission color.

We tested this hypothesis, by applying a gate terminal on top of the graphene/SiO_2/p-GaN stack that resulted in the selective modulation of graphene's Fermi level and the blocking of tunneling from states in the p-GaN below that energy. First of all, we demonstrate the transfer characteristics of the transistor effect by showing that the source–drain current can be modulated by a gate voltage as shown in the Supporting Information, Figure S1. It is worth noting here that the graphene monolayer plays several important roles in our device. Because of its good conductivity and transparency, it can serve as an excellent

 © 2016 WILEY-VCH Verlag GmbH & Co. KGaA, Weinheim

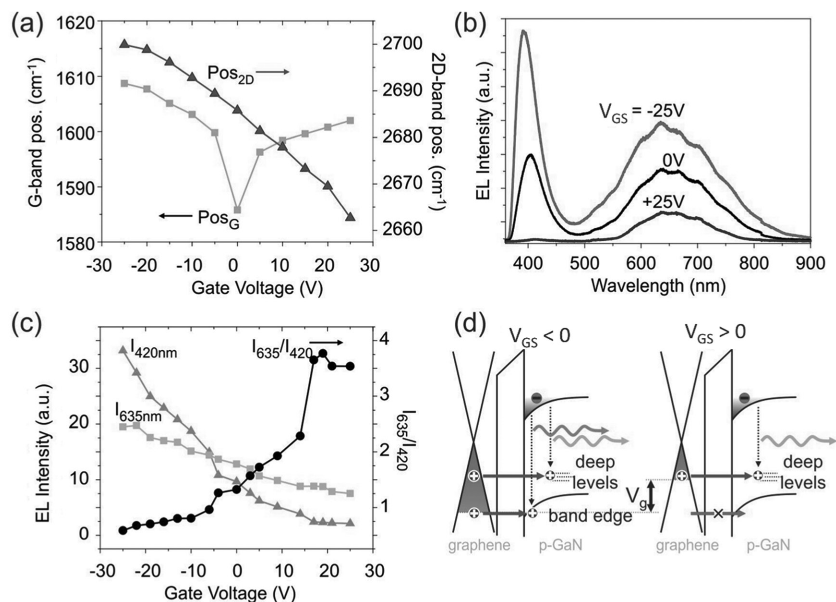

Figure 3. a) Raman position of characteristic graphene peaks (2D & G band) on p-GaN under varying gate voltage. b) Electroluminescence spectra under reverse bias for different applied gate voltages. c) Intensity (left axis) and ratio (right axis) of peaks at 420 and 635 nm versus different gate bias under reverse bias. d) Schematic of carrier transport and resulting luminescence under different gating conditions.

transparent electrode. Due to its inherent nature of a monolayer, the density of states is very small, which enables to tune the Fermi level easily by an applied gate voltage. Therefore, it leads to manipulation of the tunneling to different energy levels and changes the emission color facilely. In addition, the small effective mass of the graphene layer is beneficial for the efficient tunneling injection.[20] Furthermore, the transferred method of the stacking graphene layer is very useful to avoid the short circuit compared with conventional methods for the deposition of the metal electrode, because during the deposition process, the metal atoms can penetrate through thin film defects without difficulty. Furthermore, using Raman spectroscopy, we can identify the progressing charge transfer from graphene as a function of gate voltage as indicated by the characteristic G-band and 2D-band shifts (**Figure 3**a) which indicates a significant Fermi-level shift of 1.2 eV.[21] Figure 3d depicts the energy level diagram of a reverse-biased device for different applied gate voltages. Under a positive gate voltage (which was defined $V_{GS} > 0$ V), the increase of graphene's Fermi level results in the blocking of band-edge acceptor states and thus decreases the intensity of emission at 420 nm. Because of the higher level of deep-acceptor states, the red emission is not strongly affected by this blocking process.

Our model is validated by the trends of the two emission peaks with applied gate voltage as shown in Figure 3b. The intensity of the 420 nm reduces more significantly as graphene's Fermi level is moved up in energy and tunneling states at the band edge become inaccessible. Consequently, emission from selected states can be turned off through application of a gate voltage and the intensity ratio of the two emission peaks can be changed (Figure 3c). In our case, the device shows an orange-red emission under positive gate voltage and a higher component of blue emission under negative gate voltage. This behavior results in a change of the device's emission color of purple, to magenta and orange-red as the gate voltage is increased (Figure 3d). This novel color tunability through application of different biasing conditions of V_{SD} and V_G represents a major advance over existing color-changing LEDs who only have one adjusting parameter and thus exhibit a limited set of colors along one line in the color space.

In **Figure 4**a, we seek to further increase the achievable color tunability by changing the UV emission into visible emission through addition of downconverting QDs. For this purpose, CdSe/ZnS QDs were coated on a glass slide and positioned onto the device as shown in the Supporting Information, Figure S2. The QDs transmittance of the CdSe/ZnS shows significant light absorption in the UV range and a stable green emission at 490 nm which makes it suitable for our goal.[22] (The PL and

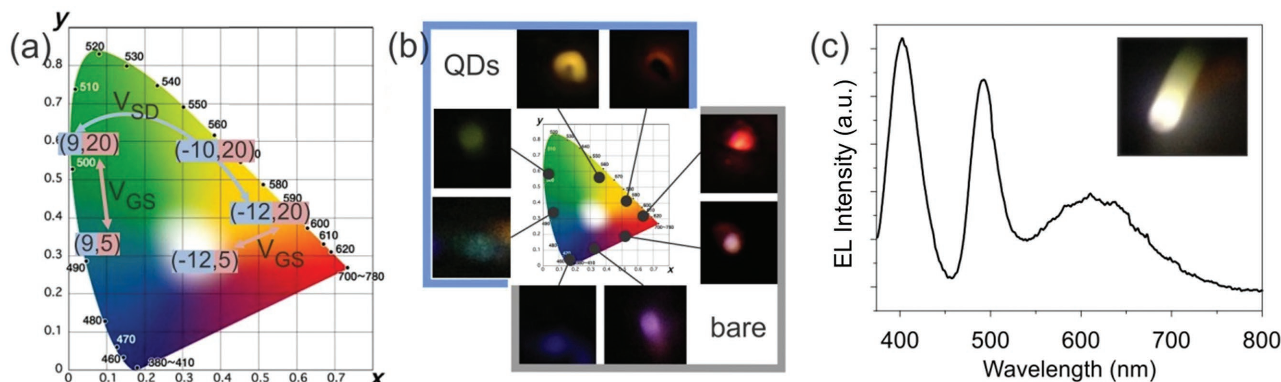

Figure 4. a) Biasing conditions (V_{SD}, V_{GS}) to access different points in the chromaticity diagram. b) Photographs of a device with and without QDs under different biasing conditions and the corresponding chromaticity points. c) EL spectrum of QD/graphene/SiO_2/p-GaN LEDs at $V_{SD} = -12$ V and $V_{GS} = -5$ V, (inset) photograph of demonstrated white light emission under those biasing conditions.

© 2016 WILEY-VCH Verlag GmbH & Co. KGaA, Weinheim

absorption spectra of QDs are shown in the Supporting Information, Figure S3.) This modification allows the control of the emission colors over a large color space as shown in Figure 4b. Separated adjustment of bias and gating allows us to traverse the color space in two independent directions indicating that any color can be emitted by this arrangement. To support this innovative aspect, we demonstrate the emission of white light and obtain the Commission Internationale de l'Eclairage (CIE) color coordinate (0.335, 0.338) by application of −12 V reverse bias and −5 V gate bias (Figure 4c).

To further investigate the feasibility of our devices, we extracted the integrated intensity of light emission under different biases and gate conditions, which is shown in the Supporting Information, Figure S4. Comparing the extracted luminous power efficiencies of our device with commercially available high brightness InGaN/GaN multiple quantum wells (MQWs) LEDs, it yields unoptimized luminous power efficiencies of ≈50% compared with the commercial device as shown in **Figure 5**. We have detected and then calculated the luminous power efficiency (lm/W), which was analyzed in line with previous works.[23,24] As shown in Figure 5a, the luminous power efficiency of our devices is about 50% of that of the commercial one under the same injection current. The power efficiency for high performance MQWs LED is around 110 lm W^{-1}, and that of our device is therefore around 55 lm W^{-1}. The result was obtained by using a rigorous measurement system of a closed integrating sphere. In terms of the calculation of input power, both of the source–drain energy consumption and the gate terminal power loss from leakage current have been included. In our case, the gate leakage current is around 10^{-9} A, which is much smaller than the source–drain current. Even though the applied gate voltage is high, it does not actually generate considerable energy consumption. One of the most important features is that the applied gate voltage can be used to modulate the emission intensity drastically, we therefore can obtain a high luminous power efficiency. As shown in Figure 5b, for the characteristic of luminescence under different bias voltage, the turn-on threshold voltage is around 3 V, which is consistent with both luminous power efficiency and source–drain current. In addition, we have plotted luminous power efficiency versus applied power as shown in the Supporting Information, Figure S5. It is clear that the result is similar to that shown in Figure 5a. We can also see that the luminous power efficiencies of the device covered with CdSe/ZnS QDs in Figure 5a are lower than the device without QDs. This result may arise from the energy loss due to the energy transfer from the emission of GaN layer to QDs. It is worth noting that the efficiency of our device can be further enhanced by reducing the thickness of the dielectric layer with a high crystalline quality, because the quantum tunneling current is exponentially proportional to the thickness of tunneling barrier. In our fabrication process, we deposited the dielectric layer by sputtering system, which can be replaced by other more advanced deposition systems, such as the atomic layer deposition method or molecular beam epitaxy. It is well-known that they are very useful to grow thin films with high quality and to avoid leakage current. Additionally, the replacement of the SiO_2 layer by a high-κ dielectric material can also improve the gating effect.

Finally, our methodology of light emitting transistor, which enables the generation and manipulation of a wide range of wavelengths covering the whole color spectrum, can be extended to many other material systems, including current commercially available inorganic and organic LEDs. For example, by the integration of a light emitting transistor on top of the conventional LEDs, with an appropriate arrangement of light emission wavelengths, one should be able to reproduce our results shown here. In addition, due to the mature technologies of the conventional organic and inorganic LEDs, it is foreseeable that our approach possesses a great potential for practical application in solid state lighting in the near future.

In summary, we have demonstrated a novel light emitting device whose emission spectrum can be modified over the whole color space by controlling the bias and gate voltages. The origin of this effect is the independent control over two emission processes, namely, band emission and deep acceptor emission. Transport measurements reveal that the combination of selective tunneling injection of carriers in certain states and the control of the emission process is the origin of this novel behavior. The emission range was increased by adding a layer of downconverting QDs and achieved color-tunability over all of the visible color space including white-light emission. These results demonstrate a universal and versatile route for energy

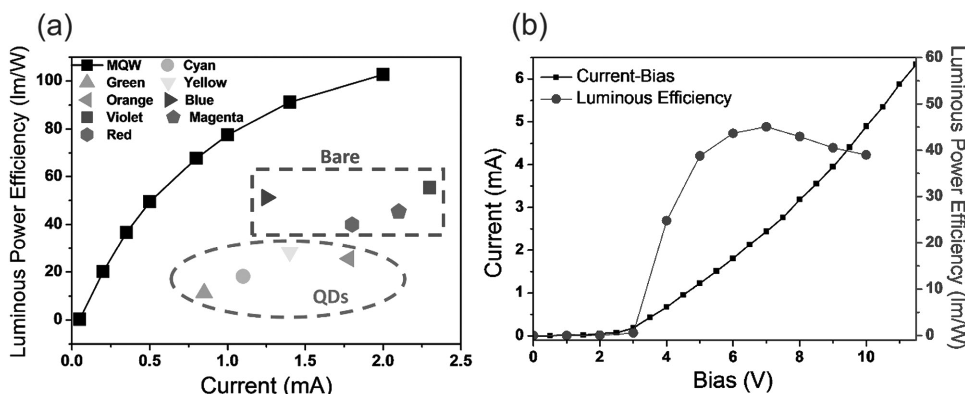

Figure 5. a) Comparison between our device and commercial high brightness InGaN/GaN multiple quantum wells (MQWs) LED for the characteristics of luminous power efficiency versus injection current under different EL conditions. b) Comparison between luminous power efficiency and source–drain current versus applied bias.

© 2016 WILEY-VCH Verlag GmbH & Co. KGaA, Weinheim

COMMUNICATION

selective light emission that is compatible with many different luminescent materials such as organic semiconductors and nanostructures and which is a promising approach for next generation optoelectronic devices.

Experimental Section

Material Preparation and *Device Fabrication*: To illustrate our working principle, the investigated light emitting devices consist of a graphene/SiO_2/p-GaN stack as shown in Figure 1a. Mg doped GaN with a doping level 3×10^{17} cm^{-3}, grown on a sapphire substrate by metal–organic chemical vapor deposition, was first cleaned using sonication. The PL spectrum under 325 nm excitation laser showed a blue emission peak at about 420 nm, which can be attributed to the interstitial Mg atoms and acceptor impurities (Figure 1b).[14] The other broadband emission at about 560 nm could be attributed to the dislocations of atoms or native point defects.[15]

Then, Ni/Au contacts were deposited and annealed to decrease their contact resistance.[25] Thin SiO_2 films were deposited on p-GaN as a tunneling barrier via RF sputtering. The graphene was grown on a copper foil via chemical vapor deposition (CVD) following previous reports.[26,27] After the CVD process, the graphene was transferred onto the SiO_2 as reported earlier.[28] The quality and characteristics of the graphene on thin SiO_2 were characterized by Raman spectroscopy (Jobin Yvon T64000), which revealed single layer properties and low defect concentrations (shown in Supporting Information, Figure S6).[29] Finally, a gate dielectric was formed on the graphene. To minimize damage to the graphene layer, we first deposited a thin SiO_2 layer (≈30 nm) by e-beam deposition and then 300 nm insulating SiO_2 layer via RF sputtering.

Supporting Information

Supporting Information is available from the Wiley Online Library or from the author.

Acknowledgements

This work was supported by the Ministry of Science and Technology and the Ministry of Education of the Republic of China.

Received: August 1, 2016
Revised: October 21, 2016
Published online: November 21, 2016

[1] H. Amano, N. Sawaki, I. Akasaki, Y. Toyoda, *Appl. Phys. Lett.* **1986**, *48*, 353.
[2] P. Waltereit, O. Brandt, A. Trampert, H. T. Grahn, J. Menniger, M. Ramsteiner, M. Reiche, K. H. Ploog, *Nature* **2000**, *406*, 865.
[3] M. R. Krames, O. B. Shchekin, R. Mueller-Mach, G. O. Mueller, L. Zhou, G. Harbers, M. G. Craford, *J. Disp. Technol.* **2007**, *3*, 160.
[4] N. Zheludev, *Nat. Photonics* **2007**, *1*, 189.
[5] S. Pimputkar, J. S. Speck, S. P. DenBaars, S. Nakamura, *Nat. Photonics* **2009**, *3*, 179.
[6] C. C. Wu, J. C. Sturm, R. A. Register, M. E. Thompson, *Appl. Phys. Lett.* **1996**, *69*, 3117.
[7] Z. L. Shen, P. E. Burrows, V. Bulovic, S. R. Forrest, M. E. Thompson, *Science* **1997**, *276*, 2009.
[8] K. Long, F. Pschenitzka, M. H. Lu, J. C. Sturm, *IEEE Trans. Electron Devices* **2006**, *53*, 2250.
[9] H. S. Tan, L. C. Chen, X. J. Wang, J. Q. Yao, C. X. Ju, H. Q. Xie, G. H. Gao, *Chin. Phys. Lett.* **1998**, *15*, 137.
[10] Y. J. Hong, C. H. Lee, A. Yoon, M. Kim, H. K. Seong, H. J. Chung, C. Sone, Y. J. Park, G. C. Yi, *Adv. Mater.* **2011**, *23*, 3284.
[11] X. M. Wang, H. Tian, M. A. Mohammad, C. Li, C. Wu, Y. Yang, T. L. Ren, *Nat. Commun.* **2015**, *6*, 6.
[12] M. Freitag, H. Y. Chiu, M. Steiner, V. Perebeinos, P. Avouris, *Nat. Nanotechnol.* **2010**, *5*, 497.
[13] Y. D. Kim, H. Kim, Y. Cho, J. H. Ryoo, C. H. Park, P. Kim, Y. S. Kim, S. Lee, Y. L. Li, S. N. Park, Y. S. Yoo, D. Yoon, V. E. Dorgan, E. Pop, T. F. Heinz, J. Hone, S. H. Chun, H. Cheong, S. W. Lee, M. H. Bae, Y. D. Park, *Nat. Nanotechnol.* **2015**, *10*, 676.
[14] M. Smith, G. D. Chen, J. Y. Lin, H. X. Jiang, A. Salvador, B. N. Sverdlov, A. Botchkarev, H. Morkoc, B. Goldenberg, *Appl. Phys. Lett.* **1996**, *68*, 1883.
[15] S. Y. Xie, Y. D. Zheng, P. Chen, R. Zhang, B. Shen, H. Chen, *Appl. Phys. A: Mater. Sci. Process.* **2002**, *75*, 363.
[16] C. W. Chang, W. C. Tan, M. L. Lu, T. C. Pan, Y. J. Yang, Y. F. Chen, *Adv. Funct. Mater.* **2013**, *23*, 4043.
[17] J. G. Simmons, *J. Appl. Phys.* **1963**, *34*, 1793.
[18] M. Depas, B. Vermeire, P. W. Mertens, R. L. Vanmeirhaeghe, M. M. Heyns, *Solid-State Electron.* **1995**, *38*, 1465.
[19] M. C. Lemme, T. J. Echtermeyer, M. Baus, H. Kurz, *IEEE Electron Device Lett.* **2007**, *28*, 282.
[20] K. S. Novoselov, A. K. Geim, S. V. Morozov, D. Jiang, M. I. Katsnelson, I. V. Grigorieva, S. V. Dubonos, A. A. Firsov, *Nature* **2005**, *438*, 197.
[21] A. Das, S. Pisana, B. Chakraborty, S. Piscanec, S. K. Saha, U. V. Waghmare, K. S. Novoselov, H. R. Krishnamurthy, A. K. Geim, A. C. Ferrari, A. K. Sood, *Nat. Nanotechnol.* **2008**, *3*, 210.
[22] B. O. Dabbousi, J. RodriguezViejo, F. V. Mikulec, J. R. Heine, H. Mattoussi, R. Ober, K. F. Jensen, M. G. Bawendi, *J. Phys. Chem. B* **1997**, *101*, 9463.
[23] X. B. Wang, X. S. Yan, W. W. Li, K. Sun, *Adv. Mater.* **2012**, *24*, 2742.
[24] M. D. Weber, L. Niklaus, M. Proschel, P. B. Coto, U. Sonnewald, R. D. Costa, *Adv. Mater.* **2015**, *27*, 5493.
[25] D. Qiao, L. S. Yu, S. S. Lau, J. Y. Lin, H. X. Jiang, T. E. Haynes, *J. Appl. Phys.* **2000**, *88*, 4196.
[26] A. Reina, X. T. Jia, J. Ho, D. Nezich, H. B. Son, V. Bulovic, M. S. Dresselhaus, J. Kong, *Nano Lett.* **2009**, *9*, 30.
[27] X. S. Li, W. W. Cai, J. H. An, S. Kim, J. Nah, D. X. Yang, R. Piner, A. Velamakanni, I. Jung, E. Tutuc, S. K. Banerjee, L. Colombo, R. S. Ruoff, *Science* **2009**, *324*, 1312.
[28] W. Regan, N. Alem, B. Aleman, B. S. Geng, C. Girit, L. Maserati, F. Wang, M. Crommie, A. Zettl, *Appl. Phys. Lett.* **2010**, *96*, 3.
[29] A. C. Ferrari, J. C. Meyer, V. Scardaci, C. Casiraghi, M. Lazzeri, F. Mauri, S. Piscanec, D. Jiang, K. S. Novoselov, S. Roth, A. K. Geim, *Phys. Rev. Lett.* **2006**, *97*, 187401.

© 2016 WILEY-VCH Verlag GmbH & Co. KGaA, Weinheim